Structure and spectroscopy of Ne_nSH $(\tilde{A}\,^2\Sigma^+)$ complexes using adiabatic diffusion Monte Carlo (ADMC)

Hee-Seung Lee, John M. Herbert,[a] and Anne B. McCoy
Department of Chemistry, The Ohio State University, Columbus, Ohio 43210

(Received 6 July 1999; accepted 31 August 1999)

Adiabatic rigid body diffusion Monte Carlo techniques are used to investigate the structure and spectroscopy of complexes of one to four neon atoms with SH $(\tilde{A}\,^2\Sigma^+)$. While these systems contain multiple low-lying minima, the ground state wave functions are well described by a neon cluster weakly interacting with SH. This structure persists in low-lying excited states, in the case of complexes of two neon atoms with SH or SD. © *1999 American Institute of Physics.* [S0021-9606(99)00544-9]

I. INTRODUCTION

A longstanding challenge in chemical physics is to draw connections between spectroscopic information about polyatomic systems and the underlying forces between the atoms of which they are composed. If the system of interest is strongly bound and the range of energies that is probed experimentally corresponds to a regime over which the vibrational dynamics is nearly harmonic, the solution to this problem is relatively straightforward.[1] In this case, the spectrum can be fit to a model Hamiltonian in which the energy levels are parameterized in terms of the number of quanta in each of the normal modes and the angular momentum operators. The form of the Hamiltonian is based on perturbation theory and direct connections can be made between the terms in the perturbative expansion and terms in the normal mode Hamiltonian.[2] On the other hand, van der Waals complexes and other weakly bound systems that display large amplitude motions can rarely be described by a simple zero-order picture. In these cases, other approaches need to be taken in order to draw these connections.

In the present study, we focus on the spectroscopy and structure of complexes of one to four neon atoms with SH $(\tilde{A}\,^2\Sigma^+)$. The NeSH system represents the most weakly bound of a family of complexes in which OH or SH in its first excited bound electronic state interacts with a rare gas atom (Kr, Ar or Ne) which has been the subject of numerous experimental and theoretical investigations.[3] Unlike the other members of this family of complexes, NeSH can be modeled as an atom interacting with a hindered rotor, and the zero-point energy (ZPE) is only $4.5\ cm^{-1}$ smaller than the barrier between the Ne–HS and Ne–SH minima on the potential.[4] In larger Ne_nSH complexes, the ZPE is expected to exceed the energies of multiple low-lying minima.

Because the Ne_nSH complexes do not present themselves with obvious zero-order models for the vibrational motions, the assignment of the associated spectra is nontrivial. By contrast, because these systems are held together by weak intermolecular interactions, model potential energy surfaces for these complexes can be approximated by the sum of the one- and two-dimensional potentials that describe each of the $Ne\cdot Ne$[5] and $Ne\cdot SH$[4] interactions.

While, in principle, this provides us with sufficient information to calculate the rotation-vibration spectra of these complexes, in practice, the fact that these are weakly bound systems with many low frequency vibrational modes makes basis set calculations on the species with more than two neon atoms prohibitively expensive computationally. To address this issue, we use a variant of the rigid body diffusion Monte Carlo (RBDMC)[6,7] that was developed by Buch and is based on the DMC algorithm first proposed by Anderson.[8,9] This approach allows us to calculate the ground state energy relative to the potential minimum of the Ne_nSH complexes with an error of 1% to 2%. While this is not as accurate as variational approaches, the numerical uncertainty in the results of RBDMC calculations is the same size as the uncertainty in the $Ne\cdot SH$ potential surface[4] and the errors introduced by neglecting higher order interactions in the pair-wise additive approximation to the Ne_nSH potential.[10] From the RBDMC simulations we can also obtain projections of the wave function onto various coordinates in order to access the structure and the rigidity of these complexes. We find that as we move from NeSH to complexes with two, three or four neon atoms, the system becomes more rigid. In fact, like the complexes of argon with HF or HCl,[11,12,7] we find that the structures are best described by a small cluster of neon atoms interacting with SH rather than individual neon atoms interacting separately. This is surprising given the relatively low barrier for isomerization among the various low-lying minima of these systems.

The relative simplicity of implementing RBDMC comes at a severe price, that it is a relaxation method and therefore can only be applied directly to obtain the energy of the lowest lying state of a particular symmetry. Recently, we have proposed an extension to the DMC approach in which a slowly varying perturbation to the Hamiltonian is introduced.[13] We refer to this procedure as adiabatic DMC

[a]Present address: Department of Chemistry, University of Wisconsin–Madison, 1101 University Ave., Madison, WI 53706.

(ADMC) because the distribution of walkers remains in equilibrium throughout the simulation. This procedure allows us to use an approximate description of the functional form of the nodal surface to calculate energies of low-lying excited states with statistical uncertainties that are comparable to those obtained for the ground state energies. In addition, ADMC can be used to calculate rotational constants and other properties that do not fall out directly from the RBDMC simulations. We have applied this approach to calculations of the energies of fundamental vibrational modes of Ne_2SH/D and from this can investigate more closely the nature of the couplings in this system. We find that the model of a neon dimer interacting with SH persists in the excited states, including the one in which one quantum of excitation is put into the neon-neon stretching coordinate.

The remainder of this paper is organized as follows. In the next section, we review DMC and describe our implementation of RBDMC and ADMC. In Sec. III, we present the results for the complexes of SH with one to four neon atoms as well as for various excitations of the Ne_2SH/D complex. Finally, we conclude in Sec. IV.

II. THEORETICAL APPROACHES

In this study, we apply diffusion Monte Carlo (DMC), first described by Anderson,[8,9] to a study of the structure and spectroscopy of Ne_nSH complexes. This approach is based on the parallel between the diffusion equation and the time-dependent Schrödinger equation, written in terms of an imaginary time variable, $\tau = it$ $(\hbar = 1)$. In this approach, the solution to the time-dependent Schrödinger equation is obtained by propagating an ensemble of walkers, each of which represents a possible configuration of the system. The walkers are allowed to diffuse through the $3N$ dimensional configuration space of the system by a random walk procedure. Here, the displacement of each atom during each time step, $\Delta\tau$, is taken from a Gaussian random distribution, the width of which is given by

$$\sigma_i = \sqrt{\frac{\Delta\tau}{2m_i}}, \tag{1}$$

where m_i is the mass of the atom. A probability for increasing the population at a given configuration is given by $e^{V_{\mathrm{ref}} - V(\mathbf{r})}$. At long imaginary times, the solution to the time-dependent Schrödinger equation approaches

$$\lim_{\tau\to\infty} \Psi = \varphi_0 e^{-E_0\tau}, \tag{2}$$

where φ_0 is the lowest energy eigenstate of the system and E_0 is the corresponding energy. This is an exponentially decaying function. Choosing V_{ref} so that a constant population of walkers is maintained is equivalent to multiplying both sides of Eq. (2) by $e^{V_{\mathrm{ref}}\tau}$, making V_{ref} an approximation to the ground state energy of the system of interest.[14]

In the present simulations, we follow Anderson[8] and Suhm and Watts[14] and take

$$V_{\mathrm{ref}} = \overline{V} - \alpha \frac{N_\tau - N_0}{N_0}, \tag{3}$$

where $\overline{V}$ provides the average potential energy of the ensemble, N_τ the number of walkers in the ensemble at time τ and α is chosen so that the fluctuations from the Monte Carlo simulation are slightly larger than the fluctuations due to the second term in Eq. (3).

A. Rigid-body DMC

One difficulty in applying the above approach to studies of weakly bound systems comes from the fact that typically the intramolecular vibrational frequencies are two orders of magnitude larger than the intermolecular frequencies. In the case of the $\tilde{A}^2\Sigma^+$ state of NeSH, the zero-point energy of SH is approximately $1000\,\mathrm{cm}^{-1}$, whereas the zero-point energy in intermolecular modes is $63\,\mathrm{cm}^{-1}$. As such, a 1% uncertainty in the zero-point energy of this system is 15% of the zero-point energy in the intermolecular degrees of freedom, which is the quantity of interest. As a result, it would be preferable to propagate the dynamics either on an adiabatic potential where the intramolecular problem has already been solved or for a fixed intramolecular geometry. Several methods have beep proposed for achieving this,[6,15] and one that is particularly successful is the rigid body diffusion Monte Carlo approach proposed by Buch.

In this approach, instead of propagating all of the atoms, we propagate the centers of mass of all of the molecules in the system and the rotational motion of all of the molecular units. While others have employed similar approaches,[6,7] we will describe briefly our implementation of this algorithm. The diffusion of the centers of mass is implemented using standard techniques, described above. The only difference is that the total mass of the diffusing unit is used to evaluate σ in Eq. (1) rather than the mass of an individual atom.

The rotational diffusion is implemented by propagating the rotation matrices that define the orientation of the principal axes of each molecule relative to the space-fixed reference frame. In this procedure, at each time step we take an infinitesimal rotation of the space-fixed coordinate system about each of the three principal axes of each of the molecules that are to remain rigid in the simulation, where the magnitude of the rotational diffusion about each of the principal axes, $\delta_{i,\alpha}$, is taken from a Gaussian random distribution with

$$\sigma_{i,\alpha} = \sqrt{\frac{\Delta\tau}{2I_{i,\alpha}}}, \tag{4}$$

and $I_{i,\alpha}$ is the moment of inertia of the ith molecule with respect to the α-axis. By careful choice of $\Delta\tau$, we ensure that the angular displacements fall in the regime of infinitesimal rotations.[16] As such, the matrix that defines the orientation of each of the molecular units is propagated as follows:

$$\mathbf{R_i}(\tau + \Delta\tau) = \mathbf{R_{i,x}}\mathbf{R_{i,y}}\mathbf{R_{i,z}}\mathbf{R_i}(\tau), \tag{5}$$

where

$$R_{i,x}R_{i,y}R_{i,z}=\begin{pmatrix} 1 & \delta_{i,z} & -\delta_{i,y} \\ -\delta_{i,z} & 1 & \delta_{i,x} \\ \delta_{i,y} & -\delta_{i,x} & 1 \end{pmatrix}. \quad (6)$$

The rotation matrices are then used to evaluate the orientation of the molecular units relative to the Cartesian coordinate axis system used in the propagation of the centers of mass.

Finally, we should note that in the case of linear molecules, the propagation will be invariant to rotation about the molecular axis and one can simplify the rotational propagation by including only rotations about two axes that are perpendicular to the molecular axis. In our implementation, we have not taken advantage of this simplification.

B. Adiabatic DMC (ADMC)

One of the largest advantages of DMC, that it provides a general algorithm to evaluate the ground state energy of the system of interest, leads to difficulties if one wants to evaluate accurate excited state energies or properties of the system other than energy, for example, $\langle W\rangle$ where W is some general operator. We have recently developed a general adiabatic extension to DMC, ADMC, which addresses both of these issues. The approach is described elsewhere,[13] and we will provide a brief summary of the key points.

In the case of evaluating expectation values of general operators, W, we use ADMC to propagate the Hamiltonian

$$H' = H^{(0)} + \lambda W, \quad (7)$$

where $H^{(0)}$ is the vibrational Hamiltonian for the system of interest and $\lambda = \lambda(\tau=0) + \Delta\lambda \times \tau$. In these simulations, the system is equilibrated for a particular value of $\lambda(\tau=0)$. Once this has been achieved, λ is allowed to increase linearly with τ so that at each time step λ is increased by a small increment, $\Delta\lambda$. In this way, the Hamiltonian is changed adiabatically throughout the simulation. If we plot V_{ref} as a function of τ it will no longer be constant. Instead, perturbation theory tells us that the lowest energy eigenvalue of the Hamiltonian in Eq. (7) can be approximated by

$$E_0' = E_0^{(0)} + \lambda\langle\psi_0^{(0)}|W|\psi_0^{(0)}\rangle + O(\lambda^2). \quad (8)$$

Therefore, if we fit $V_{\mathrm{ref}}(\lambda)$ to a low order polynomial in λ, the constant contribution is the lowest eigenvalue of the unperturbed Hamiltonian and the linear term provides $\langle W\rangle$. For each of the reported energies, we run five simulations with different initial conditions, and obtain E_0 by taking an intercept of the fit to Eq. (8). The reported energies and uncertainties represent the average of these simulations. Typically, the Monte Carlo simulations lead to uncertainties in the results that are approximately 1% of the calculated energy. An example of the raw results of such a simulation is plotted in Fig. 1(a).

We employ a similar approach to determine the location of nodes in the simulations for excited vibrational states when their functional form is known. Here we use a fixed node approximation in which any replica that crosses the node will be removed from the simulation.[9] In this way, we calculate the energy based on the wave function on one side of the node. This is relatively easily implemented when the location of the node is known by symmetry. When this is not the case, the situation becomes more complicated. A general procedure for calculating excited states, proposed by Coker and Watts, imposes the condition that the calculated wave functions are orthogonal.[17] Alternatively, Buch and coworkers have demonstrated that excited state energies can be calculated using DMC when one requires that the energies, calculated on the two sides of the node, are equal, and the wave function be continuous with a continuous first derivative.[18] Even within these constraints, it is often difficult to determine the precise location of the nodal surface as statistical fluctuations in $V_{\mathrm{ref}}(\tau)$ can be large. In some cases, including the Ne_nSH complexes considered in the present study, one can generate a set of approximate nodal surfaces that are simple functions of the internal coordinates of the system of interest, where the approximate location of the nodal surface depends on the values of a small number of parameters $\{\eta\}$. In the present case, we use a single parameter and define the nodal surface by $F(\mathbf{x})=\eta$. Here, $\mathbf{x}$ represents the coordinates that are being propagated in the RBDMC simulation and $F(\mathbf{x})$ is the function of these coordinates that defines the shape of the nodal surface. In the ADMC procedure, we perform two simulations in which η is varied linearly with τ, one on each side of the node. The resulting plots of energy as functions of η are fit to low order polynomials. The value of η at which the two curves cross provides the position of the nodal surface and the corresponding energy. An example of the raw results of such a simulation is plotted in Fig. 1(b).

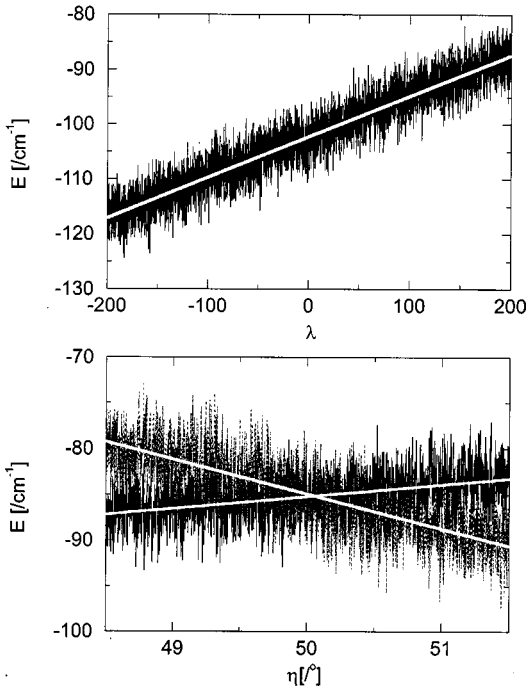

FIG. 1. The raw results from ADMC runs that are used to calculate (a) the B rotational constant for Ne_2SH and (b) the energy of the wagging vibration of Ne_2SH.

TABLE I. Energies and rotational constants for low-lying minima of the Ne_nSH potentials.

System	E^a_{min} (/cm^{-1})	A (/MHz)	B (/MHz)	C (/MHz)	Description, point group symmetry
NeSH	−103.7		2815.3		Linear Ne–HS, $C_{\infty v}$
	−87.9		3926.7		Linear HS–Ne, $C_{\infty v}$
Ne_2SH	−197.7	5556.9	2299.8	1626.6	T-shaped, Ne_2–HS, C_{2v}
	−191.9		1020.7		Linear Ne–Hs–Ne, $C_{\infty v}$
	−167.7	5518.5	2927.8	1912.9	T-shaped HS–Ne_2, C_{2v}
Ne_3SH	−322.7	2734.9	1501.7	1501.7	Tetrahedral Ne_3–HS,[b] C_{3v}
	−286.3	5556.3	797.2	697.2	T-shaped Ne_2–HS–Ne, C_{2v}
	−281.6	2716.5	1757.5	1757.5	Tetrahedral HS–Ne_3,[b] C_{2v}
Ne_4SH	−430.9	1499.2	1434.6	1003.3	Equatorial SH, C^c_{2v}
	−417.9	2722.8	898.4	898.4	Axial SH, C^c_{3v}

[a]Energies of the minima relative to the dissociated cluster.
[b]In these complexes, the neon atoms from an equilateral triangle.
[c]In these complexes, the four neon atoms and the SH from a trigonal bipyramidal structure with the SH in either an equatorial or an axial position.

C. Recrossing correction

In order to improve the accuracy of the excited state energies, we have incorporated a recrossing correction. In this correction, the possibility that a given replica crosses the nodal surface and back in a single time step is evaluated in order to remove these replicas from the ensemble. Following Anderson,[9] this probability is given by

$$P_{ex}=\exp\left(\frac{-2x(\tau)x(\tau+\delta\tau)}{\sigma^2}\right), \tag{9}$$

and is compared to a random number between zero and one. If the probability is larger than the random number, the replica is removed from the ensemble.

In the case of multidimensional RBDMC simulation, the correction becomes nontrivial to implement mainly because we have to deal with the rotation as well as the translational motion. Sandler, Buch and Sadlej have shown that a multidimensional generalization of Eq. (9) can be achieved by introducing scaled coordinates, $q_i=x_i/\sigma_i$.[18] This scaling of the coordinates allows us to treat translation and rotational motion equivalently. In these coordinates, the probability for recrossing becomes,

$$P_{ex}=\exp(-2s(\tau)s(\tau+\delta\tau)), \tag{10}$$

where s represents the distance of a walker from the nodal surface in the scaled coordinates, where

$$s=\frac{\|\mathcal{F}(\mathbf{q})\|}{\|\nabla\mathcal{F}(\mathbf{q})\|}. \tag{11}$$

Here $\mathcal{F}(\mathbf{q})=\eta$ defines the nodal surface in the scaled coordinates, and the derivatives in the denominator are taken in the scaled coordinates. Calculating $\|\mathcal{F}(\mathbf{q})\|$ is straightforward and the gradient in scaled coordinate is obtained using the chain rule,

$$\frac{\partial\mathcal{F}(\mathbf{q})}{\partial q_i}=\sigma_i\frac{\partial F(\mathbf{x})}{\partial x_i}. \tag{12}$$

When the nodal surface depends only on distances between the molecular units, evaluation of the derivative in Eq. (12) is straightforward. However, in the case of bending vibration of SH, evaluation of the recrossing correction becomes more complicated because rotational motion of SH must be included. In these cases, the derivatives in Eq. (12) are evaluated using a second order finite difference scheme.

D. Potential energy surface

In this study, the potential energy surfaces for the Ne_nSH complexes are approximated by the sum of the Ne·Ne (HFD-B) potential of Aziz[5] and the Ne·SH potential developed recently by us.[4] The HFD-B neon dimer potential represents a fit to a range of experimental data, including the virial coefficients, viscosity, conductivity and scattering cross sections. The potential energy surface for NeSH was obtained by fitting ten band origins and rotational constants of NeSH and NeSD, obtained from the high-resolution laser-induced fluorescence spectra.[4] The functional form used for the potential is the same as that used by Hutson to fit the ArHCl potential.[19] The band orgins and rotational constants for NeSH and NeSD, calculated using this potential, are within 1% of the experimental values. The potential has a minimum at $-103.7\,\mathrm{cm}^{-1}$, in the Ne–H–S geometry, and at $-87.9\,\mathrm{cm}^{-1}$, in the Ne–S–H geometry. These minima are separated by a $67.1\,\mathrm{cm}^{-1}$ barrier, measured relative to the global minimum, which is peaked at $\theta=82.5°$.

The global minimum and several local minima of each of the Ne_nSH ($n\leqslant 4$) systems have been located by the down-hill simplex minimization scheme,[20] with an initial geometry chosen to be close to one of the expected minima. The energies and corresponding rotational constants of several low-lying minima of the Ne_nSH complexes with $n\leqslant 4$ are listed in Table I. In all cases, the energy differences between these local minima are smaller than the zero-point energy (ZPE) of NeSH.

The minimum energy structures for each size complex are depicted in Fig. 2. For the NeSH complex, the energy difference between the Ne–HS and Ne–SH minima is only $15.8\,\mathrm{cm}^{-1}$, whereas the zero-point energy of this system is $62.6\,\mathrm{cm}^{-1}$, only $4.5\,\mathrm{cm}^{-1}$ below the barrier that separates the two minima. Variational calculations on this complex have shown that in spite of the large zero-point energy, the

ground state wave function remains localized in the global Ne–HS minimum.[4] The global minima for the complexes of SH with two, three or four neon atoms, all correspond to the SH being aligned along the axis that connects the centers of mass of SH and the neon complex, R_{com}, with the hydrogen end of SH pointing toward the neon atoms. In the case of the Ne_2SH and Ne_3SH complexes, shown in Figs. 2(b) and 2(c), the neon atoms form a symmetric complex. When there are two neon atoms, they lie on a line that is perpendicular to R_{com}. When three neon atoms are present, they form an equilateral triangle in the plane perpendicular to R_{com}. An alternative interpretation of the Ne_3SH complex minimum energy geometry is to consider the system as a distorted tetrahedron with the SH forming one vertex and the three neon atoms, the remaining three. In the case of Ne_4SH, the minimum energy geometries can be interpreted as a substituted distorted trigonal bipyramidal structure. The lowest energy configuration corresponds to neon atoms at both of the axial positions and two of the three equatorial positions. The structure in which SH is in an axial position is $13\,cm^{-1}$ higher in energy. These structures are plotted in Figs. 2(d) and 2(e). As was the case for NeSH, we expect all of the potential minima given in Table I to be lower in energy than the zero-point energy of the complex. The relative importance of the various minima will be determined by the rigid body ADMC simulations.

Before we discuss these results, we need to define several coordinates that will facilitate descriptions of the motion of Ne_nSH in the complexes. In addition to R_{com}, we use R_i to represent the distance of a Ne atom from the center of mass of SH and r_j to represent a Ne–Ne distance. The most important angle is the angle between $\mathbf{R}_i$ and the SH axis, θ_i, where $\theta=0$ corresponds to linear Ne_i–HS geometry. In the case of Ne_2SH, the angle between $\mathbf{r}$ and $\mathbf{R}_{com}$ is useful and is represented by χ. Another important angle in Ne_2SH and Ne_3SH is Θ, the angle between two of the $\mathbf{R}_i$. In planar geometry, $\Theta=\theta_1+\theta_2$, but in general, $\Theta<\theta_1+\theta_2$.

III. RESULT AND DISCUSSION

A. Ground state properties of Ne_nSH ($n=1-4$)

Ground state energies and rotational constants of Ne_nSH ($n=1-4$) clusters have been calculated using ADMC, as detailed in the previous section. In the calculations of the rotational constants, a 100 a.u. time step is used. After the system is equilibrated for the initial value of λ, the simulations are run for 8000 time steps. For all of the simulations, the linear term in Eq. (8) is obtained by a linear fit of the raw data which is similar to the data plotted in Fig. 1(a). The reported values for the rotational constants represent the average of five simulations, and the uncertainties, the standard deviation of these runs.

A question that has been of recent interest involves the appropriate embedding of the body-fixed axis system and definition of the vibrationally averaged rotational constants for floppy systems.[18,21] Optimally, one would like to use the definition for which the rotational and vibrational motions are most nearly separable in order to provide a close approximation to the experimentally derived rotational constants. In practice, the calculated vibrationally averaged rotational constants for the ground state are often insensitive to the choice of embedding, at least within the accuracy that can be achieved by ADMC simulations.

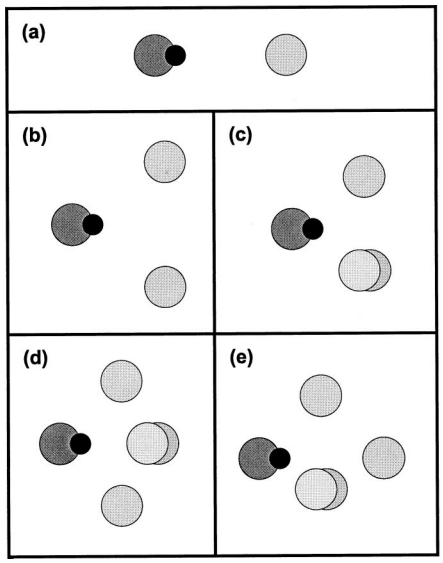

FIG. 2. Minimum energy geometries of the Ne_nSH complexes for $n=$(a) 1, (b) 2, (c) 3 and (d) 4. A second low-lying minimum of the Ne_4SH complex is shown in panel (e).

In the present simulations, we employ two approaches to calculate the rotational constants. In the first, we define a body-fixed principal axis system in which the z-axis is chosen to lie along R_{com}. The y-axis is chosen so that the neon cluster is symmetric with respect to reflection in the yz-plane. For the Ne_2SH complex, this axis corresponds to r, for Ne_3SH the axis connects one neon atom to the center of mass of the other two, while in Ne_4SH the axis connects the two *axial* neon atoms in Fig. 2(d). The moment of inertia tensor is calculated using the above choice of embedding and the rotational constants are obtained from the diagonal elements of the inverse of the moment of inertia tensor. In the case of Ne_2SH, analytical expressions for the rotational constants can be obtained,[22] while for larger complexes, the rotational constants are calculated numerically. In the second approach, we diagonalize moment of inertia tensor for each walker configuration at a given time and use the reciprocal of the eigenvalues to determine the rotational constants at that configuration.[18] In Table II, we report the rotational constants, calculated using an embedded axis system for Ne_2SH/D and Ne_3SH and using the instantaneous inertial axes to determine the rotational constants for Ne_2SH and Ne_4SH. Comparing the rotational constants for Ne_2SH, calculated by the two methods, we find that the differences are less than 50 MHz and that, in all cases, the error bars for the rotational constants calculated by the two approaches overlap.

The apparent insensitivity of the calculated rotational constants to the choice of embedding of the principal axis system will break down if the ground state has significant probability amplitude in regions of the potential of where two or more of the rotational constants are approximately

TABLE II. Energies, rotational constants and zero-point energies for Ne_nSH/D complexes.

System[a]	D_0[b] (/cm^{-1})	%[c]	$\langle A\rangle$[b] (/MHz)	$\langle B\rangle$[b] (/MHz)	$\langle C\rangle$[b] (/MHz)
NeSH[d]	−41.11(0.08)	60.0		2653(17)	
Ne_2SH[d]	−102.36(0.05)	48.2	4853(48)	2211(19)	1502(10)
Ne_2SH[e]	−102.38(0.11)	48.2	4896(21)	2164(25)	1493(23)
Ne_2SD[d]	−112.70(0.04)	43.0	4989(40)	2146(10)	1477(10)
Ne_3SH[d]	−182.27(0.12)	43.5	2369(20)	1384(14)	1375(8)
Ne_4SH[e]	−257.20(0.20)	40.3	1427(21)	1212(21)	963(21)

[a]7000 walkers were used in the simulation of NeSH while 10 000 walkers were used in the simulations of the larger complexes. In the calculations of the rotational constants, the simulations were run for 8000 time steps over which λ in Eq. (7) was varied from −200 to 200, except in simulations of the $\langle A\rangle$ for Ne_2SH, where λ ranged from −50 to 50, $\langle A\rangle$ for Ne_3SH, where λ ranged from −120 to 120.
[b]The number in parentheses is one standard deviation.
[c]The percent difference between D_0 and D_e given in Table I.
[d]The rotational constants are calculated using analytical expressions, described in the text.
[e]The rotational constants are calculated by diagonalizing the moment of inertia tensor for each walker configuration.

equal. In these cases, the inertial axes become ill-defined, and calculations of the rotational constants using the instantaneous inertial axes will lead to unphysical results. This is the case for the Ne_3SH complex where the minimum energy configuration has C_{3v} symmetry. In this case, using instantaneous moments of inertia to calculate the rotational constants results in different values for the B and C rotational constants.

The calculated rotational constants are reported in Table II as well as the ground state energies of each of the clusters. As the form of Eq. (8) indicates, the ground state energy of the unperturbed system, $E_0^{(0)}$, is given by the constant term in the fits of the ADMC simulations of the rotational constants. Therefore, the energies, reported in Table II, represent the average of 15 intercepts obtained from the rotational constant simulations and the uncertainties represent the standard deviation of these runs.

Comparing the rotational constants calculated for various minimum energy configurations, given in Table I, to the zero-point averaged rotational constants in Table II, allows us to begin to investigate the structures that dominate the ground state wave function. In the case of the complexes of two or three neon atoms, the relative sizes of the zero-point averaged constants are consistent with structures in which all of the neon atoms are at one end of the complex. In both cases, the zero-point averaged values for the constants are closer in value to those calculated for the minimum energy structure in which the hydrogen end of SH is pointing toward the neon complex. In the case of Ne_4SH, the zero-point averaged rotational constants are consistent with the wave function being localized in the global minimum of the potential in which the complex has, on average, a C_{2v} point group symmetry.

In addition to energies and rotational constants, Table II contains the percent difference between D_0 and D_e for these complexes. These numbers can be better thought of as the percent of the dissociation energy of the system that goes into zero-point energy. It is apparent from these results that the ZPE represents a considerable fraction of well depth, D_e. In most cases it is about 45% of well depth, with an exception of the NeSH system, where it is 60%. In fact, comparison of the D_0 in Table II to the corresponding energies of local minima on the surface shows that the ground state is located at an energy that is higher than at least two minima on the potentials for Ne_nSH for $n \leqslant 4$. A similar, but less dramatic, decrease in the fraction of the well-depth that is taken up by the ZPE has been reported previously for other rare gas XH complexes, for example Ar_nHF.[7]

The normalized distributions of walkers along various geometric parameters that describe the ground states of the Ne_nSH complexes are plotted in Fig. 3. In the present context, these distributions can be considered as one-dimensional projections of the total wave function onto the particular coordinate of interest.

Focusing on Figs. 3(a) and 3(b), we find that the structure of the Ne·SH moiety persists as the complex increases in size. This is most clearly illustrated in the distributions of walkers that correspond to the distances between each of the

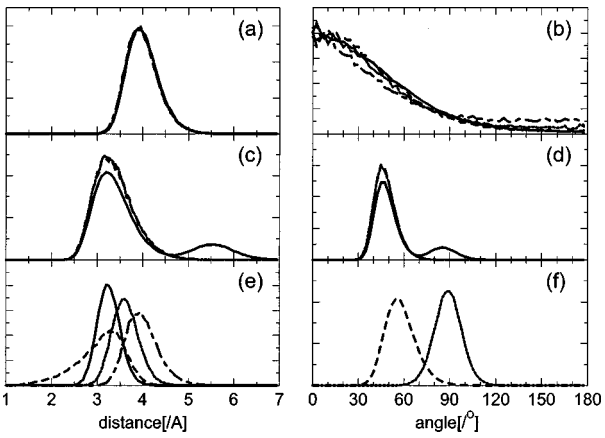

FIG. 3. The total wave functions for the ground state of NeSH (dot-dashed line), Ne_2SH (dotted line), Ne_3SH (dashed line) and Ne_4SH (solid line) are projected onto (a) R, (b) θ, (c) r, (d) Θ, (e) R_{COM}. Here, R represents the Ne–SH distances, r the Ne–Ne distances and R_{COM} the distance between the centers of mass of SH and the neon cluster. The angles between the R and the SH bond are given by θ, and Θ represents the Ne–SH–Ne angles. In panel (f), we plot the projections of the wave function for Ne_2SH onto the angle between r and R_{com} with a dotted line, and the angle between the two r vectors in Ne_3SH is plotted with a dashed line.

neon atoms in the complex and the center of mass of SH, plotted in panel (a). Here, the distributions are essentially identical for all four cluster sizes. Differences are more apparent in the distributions of the Ne–S–H angles, θ, plotted in Fig. 3(b), but even here the distributions are qualitatively insensitive to the number of neon atoms present. The most striking change in these distributions can be seen at large angles where the projection of the wave function decreases with increasing complex size. This indicates that the SH bending vibration becomes more localized in the Ne–H–S geometry as the number of neon atoms increases, a result that is consistent with the complexes mainly sampling the minimum energy structures shown in Fig. 2.

Similar trends are observed for the Ne–Ne distributions, plotted in Figs. 3(c) and 3(d). Here the distributions do not change dramatically between the Ne_2SH and the Ne_3SH complexes. The peaks in these distributions also correspond well with the larger peak in the Ne_4SH distribution. In addition, the peaks at 3.25 Å in Fig. 3(c) exactly overlap the ground state wave function for neon dimer. As with the Ne·SH moieties, the structure of the neon dimer persists in larger complexes. This result is somewhat surprising because it implies that the neon dimer retains its identity in the complex with the SH radical even though the Ne·SH interaction is much stronger than the Ne·Ne interaction. This behavior is further supported by the similarity of the distributions in the Ne–SH–Ne angle, Θ, plotted in Fig. 3(d), to those plotted in Fig. 3(c) for r. These results clearly indicate that the neon atoms are not moving independently. Instead they behave like a unit within the complex.

In Ne_4SH, the picture is a bit more complicated, as is indicated by the second peak in Figs. 3(c) and 3(d). The areas under these peaks are one-fifth those of the larger peaks in the plots and this 1:5 ratio is consistent with the Ne_4SH structure plotted in Fig. 2(d). Here there are six Ne–Ne distances, five of which are the same, while the distance between the two neon atoms in axial positions should be a factor of $\sqrt{3}$ times longer than the others. This is approximately the ratio of the positions of the centers of the two peaks in Figs. 3(c) and 3(d). If the SH had substituted at an axial position in the Ne_4SH complex, as is depicted by Fig. 2(e), we would have expected all of the Ne Ne distances to be the same, and if the ground state of the Ne_4SH complex sampled both minima, the ratio between the two peaks in Figs. 3(c) and 3(d) would be smaller than 1:5. As with the smaller complexes, these results are consistent with the SH interacting with a neon complex.

The structures of the Ne_2SH and Ne_3SH complexes are further supported by the distributions plotted in Fig. 3(f). For Ne_3SH, we have plotted the distribution of walkers for the Ne–Ne–Ne angle with a dashed line. Since this distribution has the maximum at approximately 60° and the distribution in the Ne–Ne distances in Fig. 3(c) contains only one peak, we conclude that the ground state wave function samples only the minimum depicted in Fig. 2(c). In the case of the Ne_2SH complex, the distribution in χ, the inclination angle of the Ne_2 unit, is plotted with a dotted line. Here the distribution is peaked around 90°, indicating a T-shaped structure of this complex, consistent with the minimum energy configuration, plotted in Fig. 2(b).

Finally, in Fig. 3(e), we plot the distributions of walkers for the distance between the centers of mass of SH and the neon complex R_{com}. In the case of NeSH, this distribution is identical to that plotted in panel (a). As the complex size increases, the distribution shifts to shorter distances and broadens. This is a reflection of the neon complex becoming more opened as the second and third neon atoms are added, and in the case of Ne_3SH the SH molecule can penetrate into the neon complex. When the fourth neon atom is added, the complex becomes more compact and while the peak in the distribution in R_{com} continues to shift to smaller distances, the distribution narrows.

B. Excited vibrational states of Ne_2SH/D

In addition to investigating the size dependence of the Ne_nSH complexes, we have made a more thorough investigation of the structure and spectroscopy of the Ne_2SH/D complex. The ground state energies and rotational constants for both of theses complexes are reported in Table II. The ground state motion of the Ne_2SD complex is similar to that of Ne_2SH. The largest differences between the wave functions for the ground state of Ne_2SD and those plotted in Fig. 3 for Ne_2SH are found in the distribution of Ne–S–H angles, plotted in Fig. 3(b). In the case of the Ne_2SD system, this distribution is much narrower. This is a reflection of the smaller rotational constant for SD, compared to SH, and the smaller zero-point energy of this isotopomer.

While a lot can be learned by studying the ground state properties of these species, it is interesting to see what happens when one quantum of excitation is put into each of the five intermolecular vibrational modes of these systems.

The transition frequencies for the five fundamental vibrational states of Ne_2SH/D are evaluated using the algorithm described in Sec. II B. The time step, $\Delta\tau$, used in these simulations is 20 a.u. In the discussion that follows, we will refer to the vibrational states by the names given by Cooper and Hutson[22] in their study of Ar_2HCl. The names, the corresponding symmetry in the C_{2v} point group, and a description of the nodal surface are given in the first two columns of Table III. The two totally symmetric modes correspond to the Ne–Ne wagging stretch and the symmetric breathing of the Ne_2SH/D complex. The χ-bend state corresponds to rotation of the neon dimer in the plane of the complex while the in-plane and out-of-plane bends correspond to rotational motion of SH.

In the calculations of the energies of those states that have B_1 or B_2 symmetry, the position of the nodal surface is determined by the symmetry, assuming that the nodal surface can be defined as a function of a single parameter. For example, in the case of the χ-bend mode, we put the node at $\chi=\pi/2$. In the case of totally symmetric states, the location of the nodal surfaces and corresponding energies are determined by ADMC. In these simulations, η is varied over 10 000 time steps with $\Delta\eta=0.000\,024$ a.u. for the calculation of the energy of the breathing stretch fundamental and $\Delta\eta=0.0004°$ for the calculation of the fundamental in the

TABLE III. Energies of the fundamental excitations of Ne_2SH/D.

State[a] (symmetry)[b]	$F(\mathbf{x})$[c]	$E^{d}_{Ne_2SH}$ ($/cm^{-1}$)	$E^{d}_{Ne_2SD}$ ($/cm^{-1}$)
Ground state (A_1)		−102.36(0.05)	−112.70(0.04)
Wagging stretch (A_1)	$\Theta=50.02°$	17.27(0.05)	18.55(0.01)
χ-bend (B_2)	$\chi=\pi/2$	19.30(0.08)	20.10(0.14)
Breathing stretch (A_1)	$R_1+R_2=7.94$ Å	25.29(0.12)	26.47(0.05)
In-plane bend (B_2)	$\theta_1-\theta_2=0$	33.41(0.06)	27.89(0.16)
Out-of-plane bend (B_1)	Molecular plane	40.83(0.05)	37.55(0.01)

[a]In naming the states we follow the notation of Cooper and Hutson (Ref. 22).

[b]The symmetries are given assuming a C_{2v} equilibrium energy configuration.

[c]The coordinates used to define the nodes are the two Ne–SH distances, R_i, the angles between R_i and the SH bond, θ_i and the Ne–SH–Ne angle Θ.

[d]The absolute energy of the ground state, E_0, and relative energies of excited states, E_n-E_0, are reported. The numbers in parentheses provide one standard deviation in the absolute energy of each state.

wagging stretch. In order to check the accuracy of our approaches, we calculate the fundamental frequencies of Ar_2HCl, where accurate energies have been reported[22]. The simulated excited state energies for Ar_2HCl are in excellent agreement with the reported values. When the recrossing correction is included, the maximum error in the ADMC results is $0.2\,cm^{-1}$ for absolute energies and $0.7\,cm^{-1}$ for the transition frequencies. This corresponds to a 2% maximum error which is comparable to the accuracy we are able to achieve in our fits of the Ne·SH empirical potential to experimental transition frequencies and rotational constants.

The energies of the five fundamental vibrational levels for Ne_2SH/D are reported in Table III. The pattern of energy levels for Ne_2SH is similar to that of Ar_2HCl[22] even though the strength of the van der Waals interactions is quite different. In Ne_2SH/D, the three lowest frequency modes correspond to motions of the neon atoms while the two highest frequency modes correspond to rotation of SH/D. This separation of frequencies is a result of the large rotational constant for SH or SD compared to the reduced mass associated with the neon vibrations. In replacing SH with SD, the frequencies of the three lowest frequency modes each increase by approximately $1\,cm^{-1}$. A similar increase in frequency upon deuteration has been seen in all of the M·XH van der Waals complexes with M=Ne, Ar, Kr and X=O, S.[23] This inverse isotope effect is a reflection of the fact that because the D_0 increases upon deuteration, the anharmonicity in the van der Waals stretch decreases slightly. In contrast, the frequency of the two high frequency modes both decrease upon deuteration. This decrease is simply a result of the smaller rotational constant of SD compared to SH, as these two excitations correlate to the doubly degenerate Π-bend, $(0,1^1,0)$, state of Ne·SH/D.

In addition to the five fundamental excitations of Ne_2SH/D that have transition energies below $50\,cm^{-1}$, we expect that energy of the state of Ne_2SH that correlates to the $(0,1^0,0)$ Σ-bend state of Ne·SH/D will also have an energy in this range. In Ar_2HCl, this state lies between the breathing stretch and the in-plane bend fundamentals and corresponds to the first overtone in the wagging stretch. Because this state is an overtone, the calculation of its energy is more complicated than that of a fundamental, since the positions of two nodes must be considered simultaneously, but we would expect that this state would lie at around $30\,cm^{-1}$ for both isotopomers.

The distributions of walkers for the five states of Ne_2SH that correspond to fundamental excitations are plotted in Fig. 4. In all cases, we use thick solid lines to plot the distributions for the walkers with $F(\mathbf{x})<\eta$ and thick dashed lines for the distributions when $F(\mathbf{x})>\eta$. By analogy to the one-

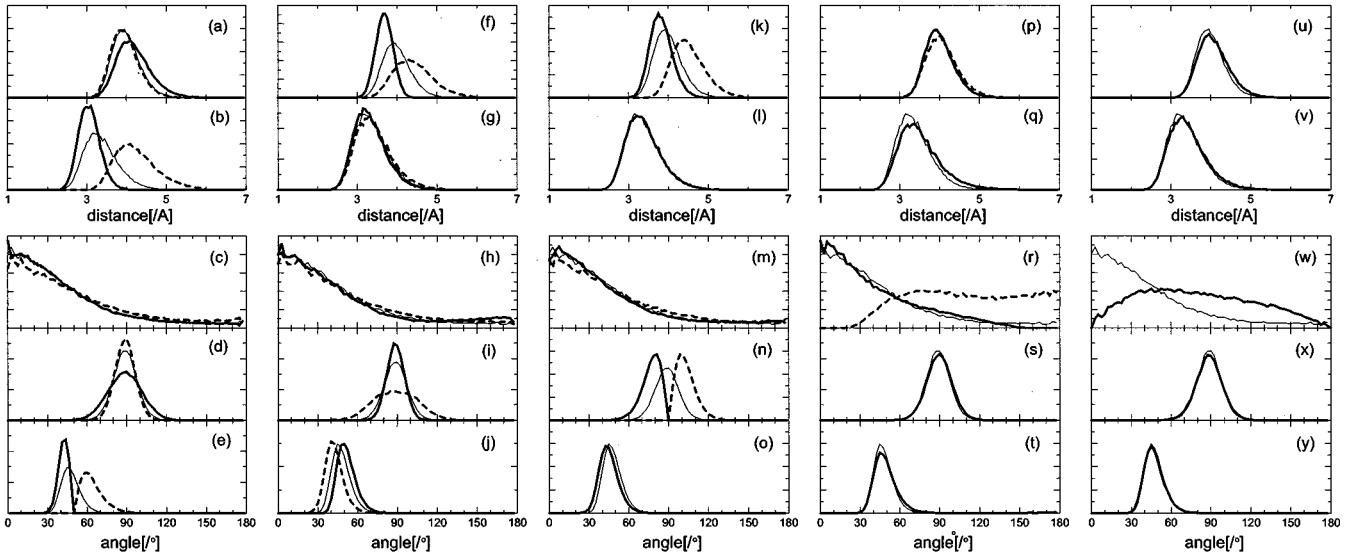

FIG. 4. The projections of the wave functions for the five fundamental excitations of Ne_2SH. In panels (a)–(e), the wave function that corresponds to the fundamental in the wagging stretch vibration is projected onto (a) R, (b) r, (c) θ, (d) χ and (e) Θ, defined in Fig. 3. In the other four columns, the fundamental in the breathing stretch [(f)–(j)], the χ-bend [(k)–(o)], the in-plane bend [(p)–(t)] and the out-of-plane bend [(u)–(y)] are projected onto these five coordinates. In this plot, thick solid and dashed lines represent the parts of the wave function on the left and right side of the node, respectively. For comparison, the corresponding distributions for ground state Ne_2SH are plotted with thin solid lines.

dimensional situation, we will refer to the two distributions as the left and right side of the node, respectively. In addition, we have plotted the ground state distribution with a thin solid line, for comparison. In the case of the three states that are not totally symmetric, a single set of simulations is performed. Since excitation in these modes removes the equivalence of the two neon atoms, the solid and dashed lines also reflect the distributions for each of the neon atoms. The wagging and breathing stretch states have A_1 symmetry and the nodal surfaces are determined by ADMC.

To begin, consider the distributions for the wagging stretch fundamental, plotted in Figs. 4(a)–4(e). In this case, the node is in Θ and the two distributions in Θ, plotted in Fig. 4(e), go to zero at the same point. In addition, these two distributions sample a larger range of angles than the ground state distribution. Further, since the Ne–Ne distance, plotted in Fig. 4(b), is closely related to Θ, the distributions for the left and right side of the nodal surface overlap over a relatively small range of r. The effects of excitation in Θ on the distributions in the other coordinates, particularly χ plotted in Fig. 4(d), are more interesting. In the case of the distribution in χ, we find that when $\Theta < 50.02°$ it is very broad, but for larger values of Θ the distribution is only slightly narrower than the ground state distribution. The observed broadening of the distribution at small χ is purely a reflection of the correlations among Θ, r and χ. When Θ decreases, either r must decrease or the Ne–Ne vector must rotate out of the T-shaped geometry. Since the Ne–Ne potential is strongly repulsive at small r, the system relaxes by rotating out of the T-shaped geometry. This in turn leads to a shift of the Ne–SH distribution, plotted in Fig. 4(a), to slightly larger distances than in the ground state.

The situation for the breathing stretch, plotted in panels (f)–(j), is similar to that for the wagging stretch fundamental. Here the coordinate of interest is the Ne–SH distance, plotted in Fig. 4(f). As before, this mode is coupled to Θ, while the coupling to r and θ is relatively small. The coupling between R and χ is similar to that seen in the wagging stretch. Here the source of the coupling is due to a decrease in the anisotropy in χ as the neon atoms move farther away from SH.

The distributions for the χ-bend state are plotted in panels (k)–(o). Since the distributions for the two neon atoms are not, in general, equivalent, we have plotted the distributions for only one of the neon atoms. One interesting feature of the distributions in r, Θ and θ comes in the similarity to the corresponding ground state distribution. In particular, the distribution in r, plotted in Fig. 4(l), is indistinguishable from the ground state distribution. This indicates that Ne_2 retains its identity as a dimer when one quantum of excitation is put into the χ-bend coordinate, and the motion that is sampled by this vibrational state corresponds to rotation of Ne_2 rather than the Ne–SH antisymmetric stretch.

The distributions of walkers for the in-plane and out-of-plane SH bending states are plotted in panels (p)–(t) and (u)–(y) of Fig. 4, respectively. As was the case for the χ-bend, the two neon atoms are not equivalent in the in-plane bend and the distributions for only one of the neon atoms are plotted here. In the case of the out-of-plane bend, the two neon atoms are equivalent. In addition, plots of the neon atom distributions on the left and the right side of the node are identical and therefore only one distribution is plotted for each coordinate. Because these states correspond to rotation of SH, only the distributions in θ, plotted in panels (r) and (w), are dramatically different from the corresponding ground state distribution. In the case of in-plane bending, the θ distributions for the left and right side of the node are not equivalent. This is a reflection of the fact that as SH rotates in the plane of the complex, one of the Ne–S–H angles will increase while the other decreases. The fact that the distribution, plotted with a dashed line, is peaked near 90° indicates that this motion is quite large amplitude. By contrast, the distribution in r, plotted in Fig. 4(q), is essentially unaffected by this excitation, indicating that the neon dimer structure persists in this excited state. Similar behavior is found in out-of-plane bending motion of SH. As is shown in Fig. 4(w), the distribution in θ is extremely delocalized, and is similar to the distribution that is obtained from the Π-bend state of NeSH. In summary, the motions associated with bending motion of SH are inherently floppy and extremely large amplitude vibrational motion, but are not, in general, strongly coupled to the other intermolecular vibrational degrees of freedom.

The distributions of walkers for the Ne_2SD fundamental vibration states are essentially the same as those for Ne_2SH, described above, with the exception of the distributions in θ. This is because the motion in this coordinate correlates with SH or SD rotation in the complex and the decrease in the rotational constant upon deuteration from 8.289 to $4.306\,cm^{-1}$ leads to a significant decrease in the amplitude of the motion in this coordinate in Ne_2SD compared to that observed in Ne_2SH. For the three lowest frequency modes of Ne_2SD, the distributions in θ vanish when $\theta \geqslant 120°$ rather than remaining finite for all angles, as was the case for Ne_2SH. In the case of the in-plane and out-of-plane bending states that correlate to the Π-bend in NeSD, more dramatic changes are observed in the θ distributions. In the case of the in-plane bending state, the distributions are shifted to the smaller angles and have very little amplitude when $\theta > 120°$. In the case of the out-of-plane bending mode, the distribution in θ is also shifted to smaller angles. Although these changes are dramatic, like the Ne_2SH complex, the distributions in θ for the Ne_2SD system correlate quite well with the corresponding distributions in NeSD.

IV. SUMMARY AND CONCLUSIONS

In this paper we have presented our approach for implementing adiabatic RBDMC and applied it to a systematic study of the structure and spectroscopy of small complexes of neon atoms with SH ($\tilde{A}^2\Sigma^+$). Although the Ne–Ne interaction is significantly weaker than the Ne·SH interaction, we find that the configurations that are sampled by complexes of up to four neon atoms with SH are localized near the global minimum. In other words, these complexes can be thought of as arising from a SH molecule interacting with a small complex of neon atoms. This is analogous to the findings of

Nesbitt and co-workers[24] in their studies of the spectroscopy of Ar_nHF complexes. In addition, in the case of complexes of Ne_2SH/D, we find that the model of a neon dimer interacting with SH or SD persists for all five fundamental vibrations. Since the Ne_n-SH complexes appear to become more rigid with increasing n, we expect that this behavior is general and would apply to the larger complexes as well.

In addition to the specific results for the complexes of neon with SH and SD, we have demonstrated a general technique for determining the structural and spectroscopic properties of weakly bound systems for which the potential energy surface can be obtained from a pair-wise sum of two and three body interactions, but where the size of the system and the fact that it can undergo large amplitude vibrations makes converged variational calculations of the rotation-vibration energy levels intractable for all but the smallest complexes. We believe that this will provide a general, systematic approach for analyzing the spectra of larger complexes of rare gas atoms with small molecules.

ACKNOWLEDGMENTS

The authors gratefully acknowledge the donors to the Petroleum Research Fund administered by the American Chemical Society, the National Science Foundation CAREER program under Grant No. CHE-9732998, and the Ohio State University Board of Regents for support of this work. J.M.H. acknowledges the REU program at Ohio State.

[1] E. B. Wilson, J. C. Decius, and P. C. Cross, *Molecular Vibrations* (Dover, New York, 1955).
[2] H. H. Nielsen, Rev. Mod. Phys. **23**, 90 (1951).
[3] C. C. Carter, T. A. Miller, H.-S. Lee, and A. B. McCoy (unpublished).
[4] C. C. Carter, T. A. Miller, H.-S. Lee, A. B. McCoy, and E. F. Hayes, J. Chem. Phys. **110**, 5065 (1999).
[5] R. A. Aziz and M. J. Slaman, Chem. Phys. **130**, 187 (1989).
[6] V. Buch, J. Chem. Phys. **97**, 726 (1992).
[7] P. Niyaz, Z. Bacic, J. W. Moskowitz, and K. E. Schmidt, Chem. Phys. Lett. **252**, 23 (1996).
[8] J. B. Anderson, J. Chem. Phys. **63**, 1499 (1975).
[9] J. B. Anderson, J. Chem. Phys. **65**, 4121 (1976).
[10] A. Ernesti and J. M. Hutson, J. Chem. Phys. **106**, 6288 (1997).
[11] S. Liu, Z. Bacic, J. W. Moskowitz, and K. E. Schmidt, J. Chem. Phys. **100**, 7166 (1994).
[12] M. A. McMahon and K. B. Whaley, J. Chem. Phys. **103**, 2561 (1995).
[13] H.-S. Lee, J. M. Herbert, and A. B. McCoy, J. Chem. Phys. **110**, 5481 (1999).
[14] M. A. Suhm and R. O. Watts, Phys. Rep. **204**, 293 (1991).
[15] A. Vegiri, M. H. Alexander, S. Gregurick, A. B. McCoy, and R. B. Gerber, J. Chem. Phys. **101**, 2577 (1994).
[16] H. Goldstein, *Classical Mechanics*, 2nd ed. (Addison-Wesley, Reading, MA, 1980).
[17] D. F. Coker and R. O. Watts, Mol. Phys. **58**, 1113 (1986).
[18] P. Sandler, V. Buch, and J. Sadlej, J. Chem. Phys. **105**, 10387 (1996).
[19] J. M. Hutson, J. Chem. Phys. **89**, 4550 (1988).
[20] W. H. Press, B. P. Flannery, S. A. Teukolsky, and W. T. Vetterling, *Numerical Recipes* (Cambridge University Press, New York, 1986).
[21] A. Ernesti and J. M. Hutson, Chem. Phys. Lett. **222**, 257 (1994).
[22] A. R. Cooper and J. M. Hutson, J. Chem. Phys. **98**, 5337 (1993).
[23] H.-S. Lee, A. B. McCoy, L. B. Harding, C. C. Carter, and T. A. Miller, J. Chem. Phys. (in press).
[24] A. McIlroy, R. Lascola, C. M. Lovejoy, and D. J. Nesbitt, J. Phys. Chem. **95**, 2636 (1991).